

Supplementary Information

Giant Enhancements in Electronic Transport and Photoelectric Properties of Bismuth Oxysulfide by Pressure-driven Layered to Three-dimensional Structural Reconstruction

Ganghua Zhang,^{*ab} Qian Zhang,^a Qingyang Hu,^a Bihan Wang^a and Wenge Yang^{*a}

^aCenter for High Pressure Science and Technology Advanced Research (HPSTAR),
Shanghai 201203, P. R. China

^bShanghai Key Laboratory of Engineering Materials Application and Evaluation,
Shanghai Research Institute of Materials, Shanghai 200437, P. R. China

**E-mail: zhangjiesss923@163.com (G.H. Zhang) and yangwg@hpstar.ac.cn (W.G. Yang)*

Contents

Figure S1. Characterization of pristine sample $\text{Bi}_9\text{O}_{7.5}\text{S}_6$ at ambient condition.

Figure S2. Typical Rietveld refinements of $\text{Bi}_9\text{O}_{7.5}\text{S}_6$ in low and high pressure phases.

Figure S3. Evolution of crystalline structure of $\text{Bi}_9\text{O}_{7.5}\text{S}_6$ before and after BiO, BiS layer buckling.

Figure S4. HRTEM micrographs of $\text{Bi}_9\text{O}_{7.5}\text{S}_6$ before and after the pressure treatment.

Figure S5. SEM and EDS mapping images of $\text{Bi}_9\text{O}_{7.5}\text{S}_6$ before and after the pressure treatment.

Figure S6. *In situ* photocurrent measurements during two sequential compression and decompression cycles.

Figure S7. *I-t* characteristic of $\text{Bi}_9\text{O}_{7.5}\text{S}_6$ during compression as a function of pressure from 0.6 to 58.1 GPa.

Figure S8. The shrinkage of $\text{Bi}(1)\text{S}_6$ octahedral layers under compression.

Figure S9. The microphotograph of the single-crystal sample in air and DAC.

Figure S10. Electronic band structure of $\text{Bi}_9\text{O}_{7.5}\text{S}_6$ during compression up to 45 GPa.

Table S1. Refined structure parameters and selected bond lengths of the $\text{Bi}_9\text{O}_{7.5}\text{S}_6$ phases at low pressure (0.5 GPa) and high pressure (25.7 GPa).

Figure S1. Characterization of pristine sample $\text{Bi}_9\text{O}_{7.5}\text{S}_6$ at ambient condition. (a) Comparison of the experimental powder XRD pattern and calculated lattice reflection planes confirms the pure $R\text{-}3m$ phase; (b) SEM and EDS characterization show the morphology of $\sim 10\text{s}$ micron sized single crystal particles and the chemical composition. The powder XRD result at ambient condition matches the literature well with hexagonal space group $R\text{-}3m$ and cell parameters $a = 4.0553(1)\text{ \AA}$, $c = 31.0177(2)\text{ \AA}$. SEM micrograph shows clearly the hexagonal plate-like morphology with a narrow particle-size distribution around $5\text{--}10\text{ }\mu\text{m}$. EDX analysis of selected regions showed a uniform composition distribution.

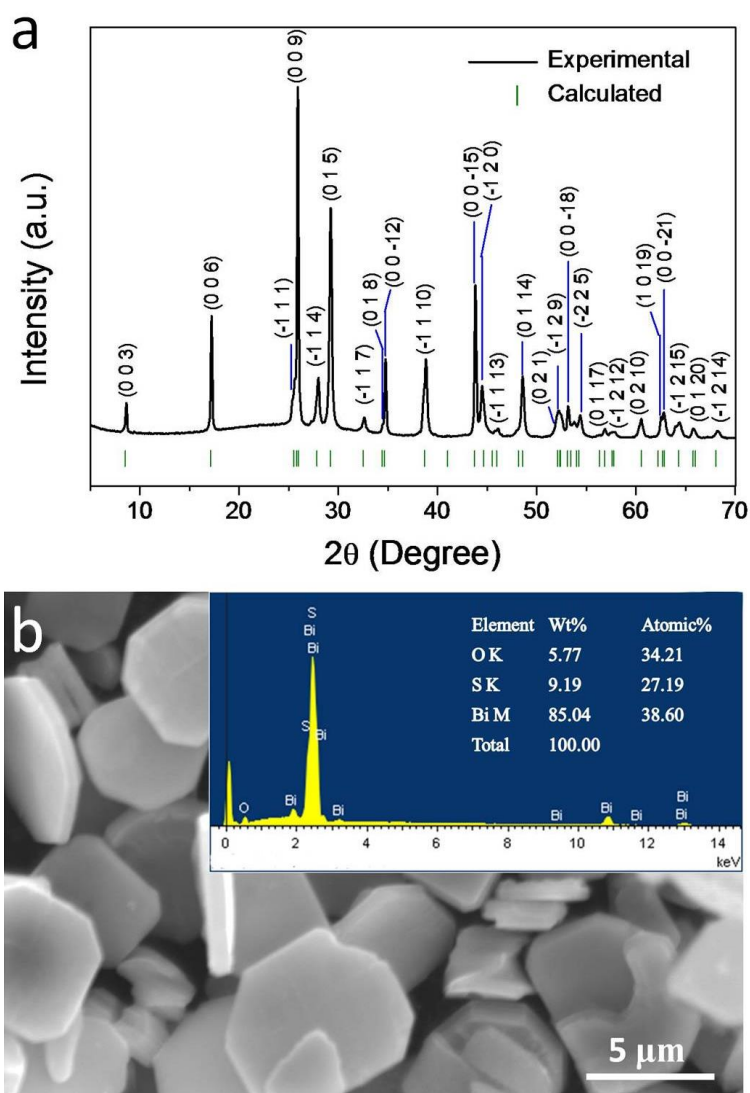


Figure S2. Typical Rietveld refinements of $\text{Bi}_9\text{O}_{7.5}\text{S}_6$ in low and high pressure phases. (a) Refinement of 0.5 GPa XRD data with space group $R\bar{3}m$, $a = b = 4.0437(2) \text{ \AA}$, $c = 30.8878(3) \text{ \AA}$ and $V = 438.83(3) \text{ \AA}^3$. (b) Refinement of 25.7 GPa XRD data with space group $R\bar{3}m$, $a = b = 3.7794(2) \text{ \AA}$, $c = 28.5252(1) \text{ \AA}$ and $V = 352.87(4) \text{ \AA}^3$.

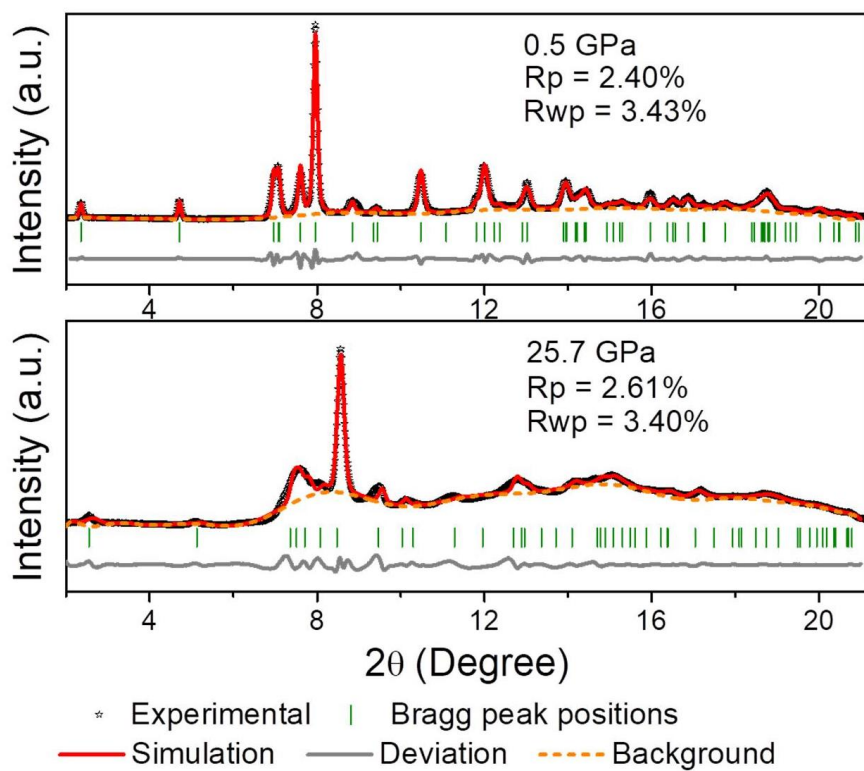


Figure S3. Evolution of crystalline structure of $\text{Bi}_9\text{O}_{7.5}\text{S}_6$ before and after BiO, BiS layer buckling. Atomic structure at ambient pressure (a) and 22.7 GPa (b) with same space group $R\bar{3}m$. The atoms are shown as balls: Bi (navy-blue), S (yellow) and O (red).

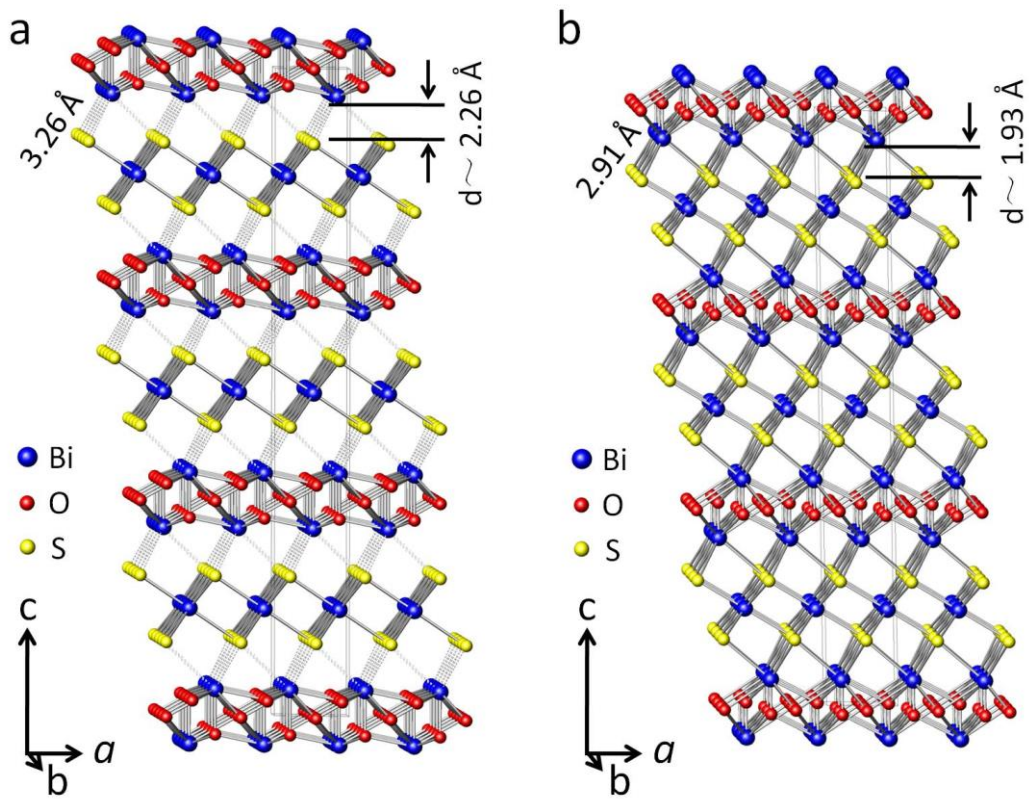


Figure S4. HRTEM micrographs of $\text{Bi}_9\text{O}_{7.5}\text{S}_6$ before (a) and after (b) the pressure treatment. The insets show the enlarged view of HRTEM image (upper right) and the electron diffraction pattern (bottom right) viewed along $[-110]$ zone axis.

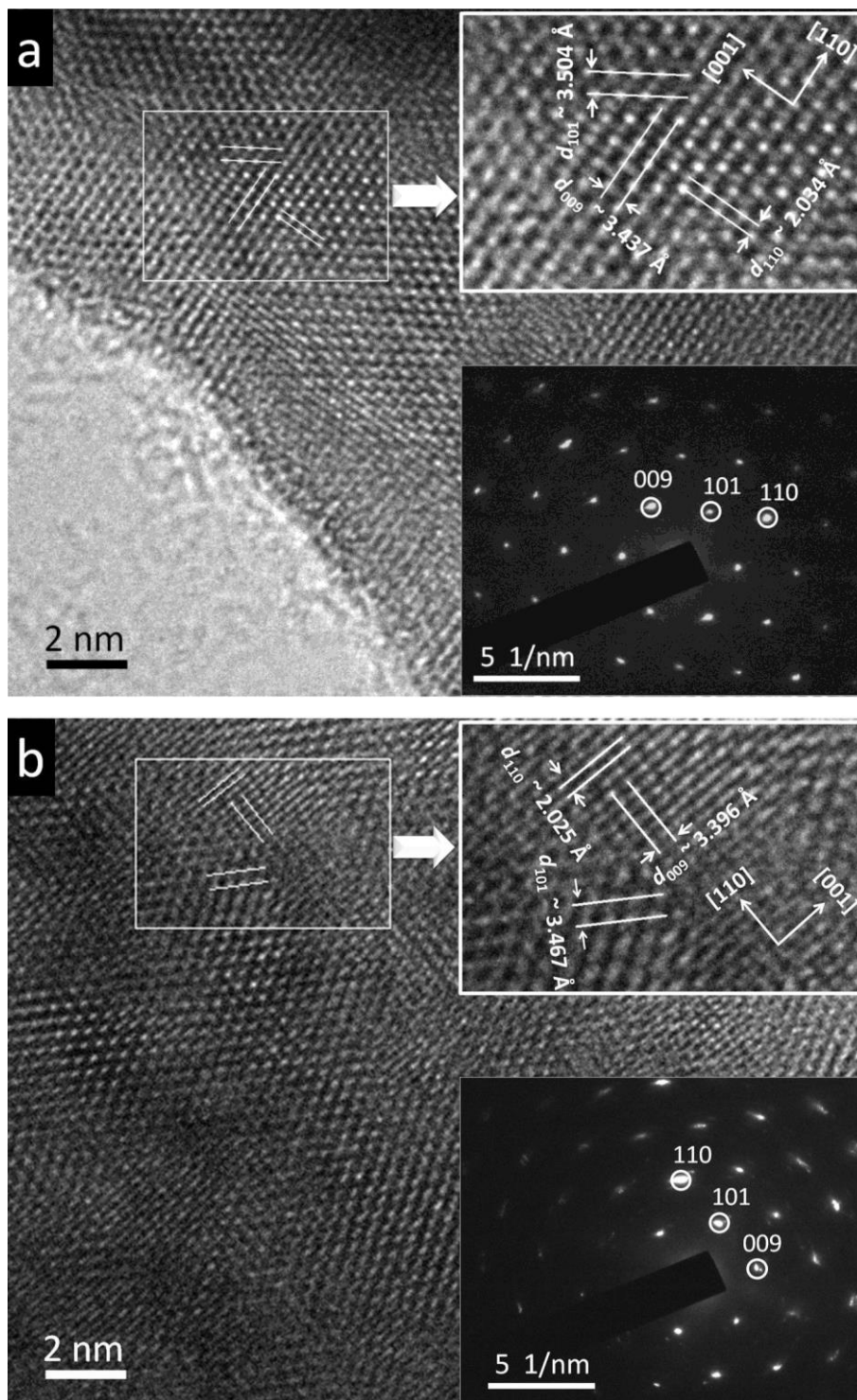


Figure S5. SEM and EDS mapping images of $\text{Bi}_9\text{O}_{7.5}\text{S}_6$ before and after the pressure treatment.

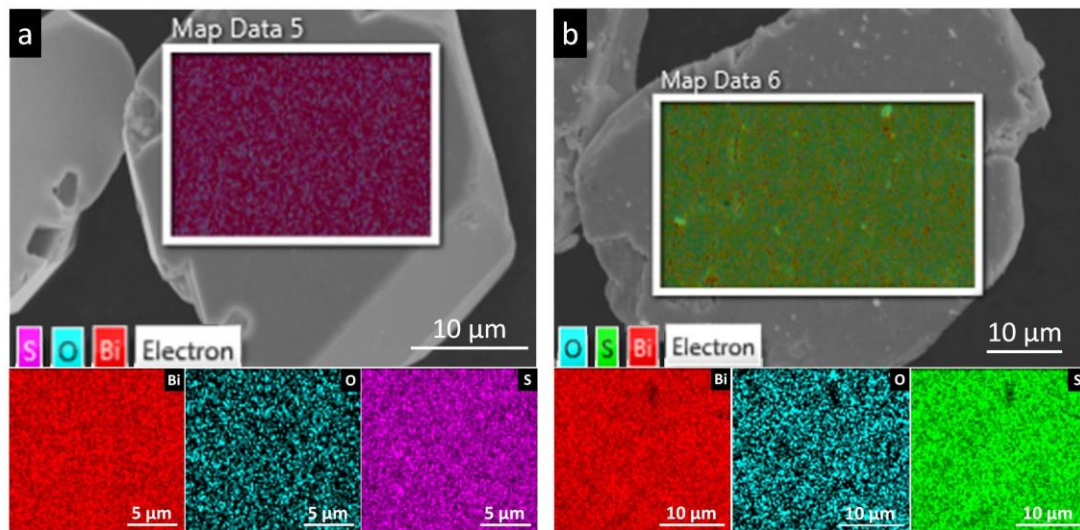


Figure S6. *In situ* photocurrent measurements during two sequential compression and decompression cycles. Photocurrent density (J_{ph}) evolution of $\text{Bi}_9\text{O}_{7.5}\text{S}_6$ up to 58 GPa (a) and enlarged view at the lower pressure region (b). Photocurrents of $\text{Bi}_9\text{O}_{7.5}\text{S}_6$ before (first cycle) and after (second cycle) pressure treatments at a low pressure of 0.6 GPa (c) and a high pressure of 58 GPa (d).

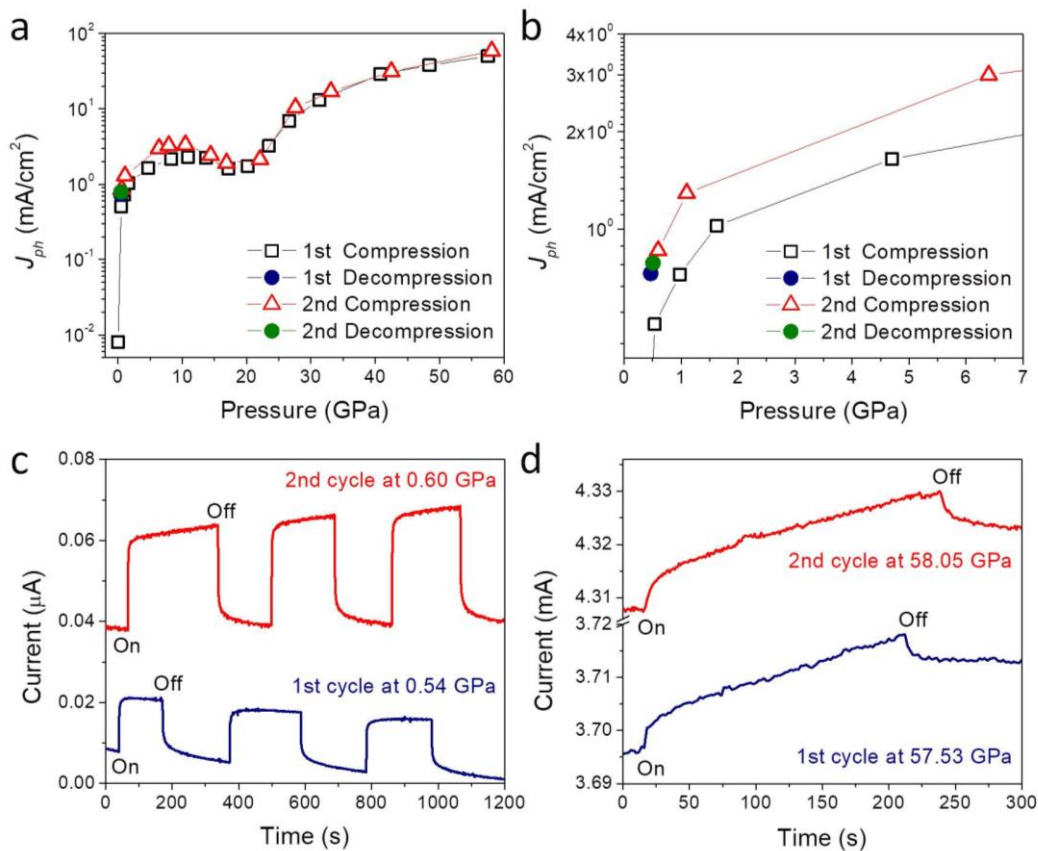


Figure S7. *I-t* characteristic of $\text{Bi}_9\text{O}_{7.5}\text{S}_6$ during compression as a function of pressure from 0.6 to 58.1 GPa.

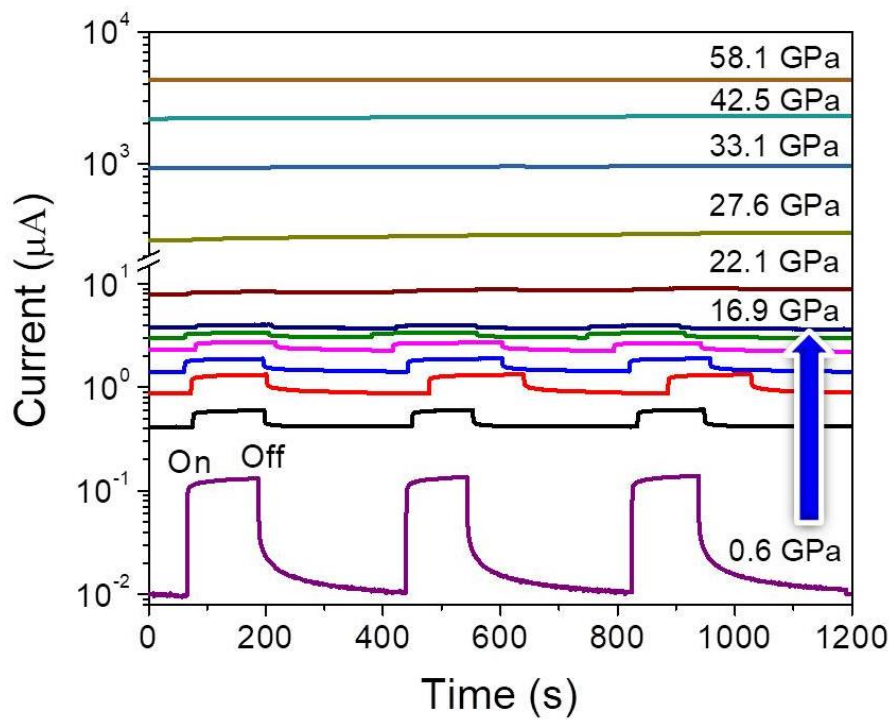


Figure S8. The shrinkage of Bi(1)S₆ octahedral layers under compression. (a) The schematic Bi-S and Bi-O layers. $d_{\text{Bi-S}}$ and $d_{\text{Bi-O}}$ indicate the thicknesses of Bi-S and Bi-O layers, respectively. (b) Normalized thicknesses of Bi-S and Bi-O layers versus pressure. The bond length of Bi(1)-S (c) and the bond angles of $\angle\text{S-Bi(1)-S}$ (d) at varied pressures.

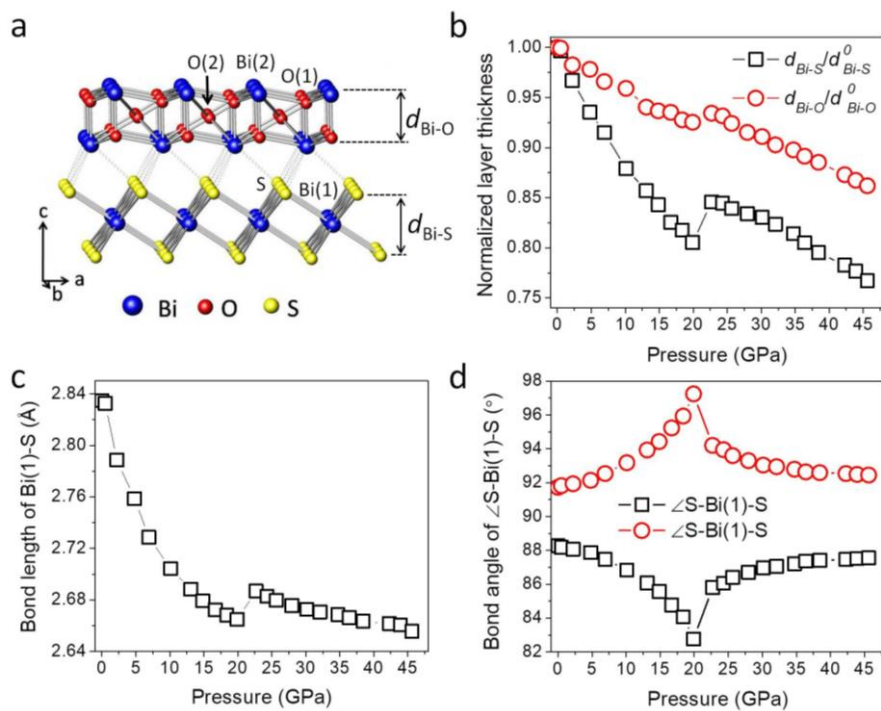


Figure S9. The microphotograph of the single-crystal sample in air (a) and DAC (b).

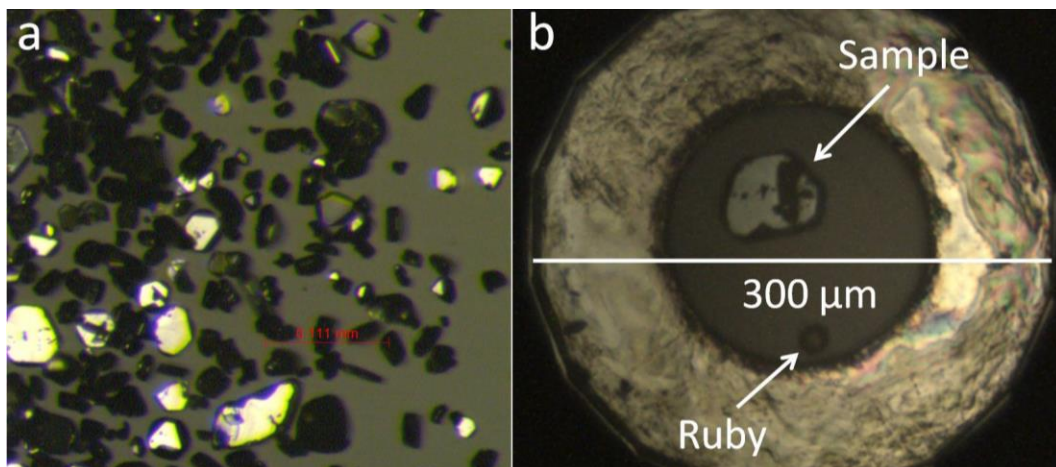


Figure S10. Electronic band structure of $\text{Bi}_9\text{O}_{7.5}\text{S}_6$ during compression up to 45 GPa. The enlarge views at Γ and A points obviously illustrate the bandgap closing and the crossover from direct to indirect-transition bandgap.

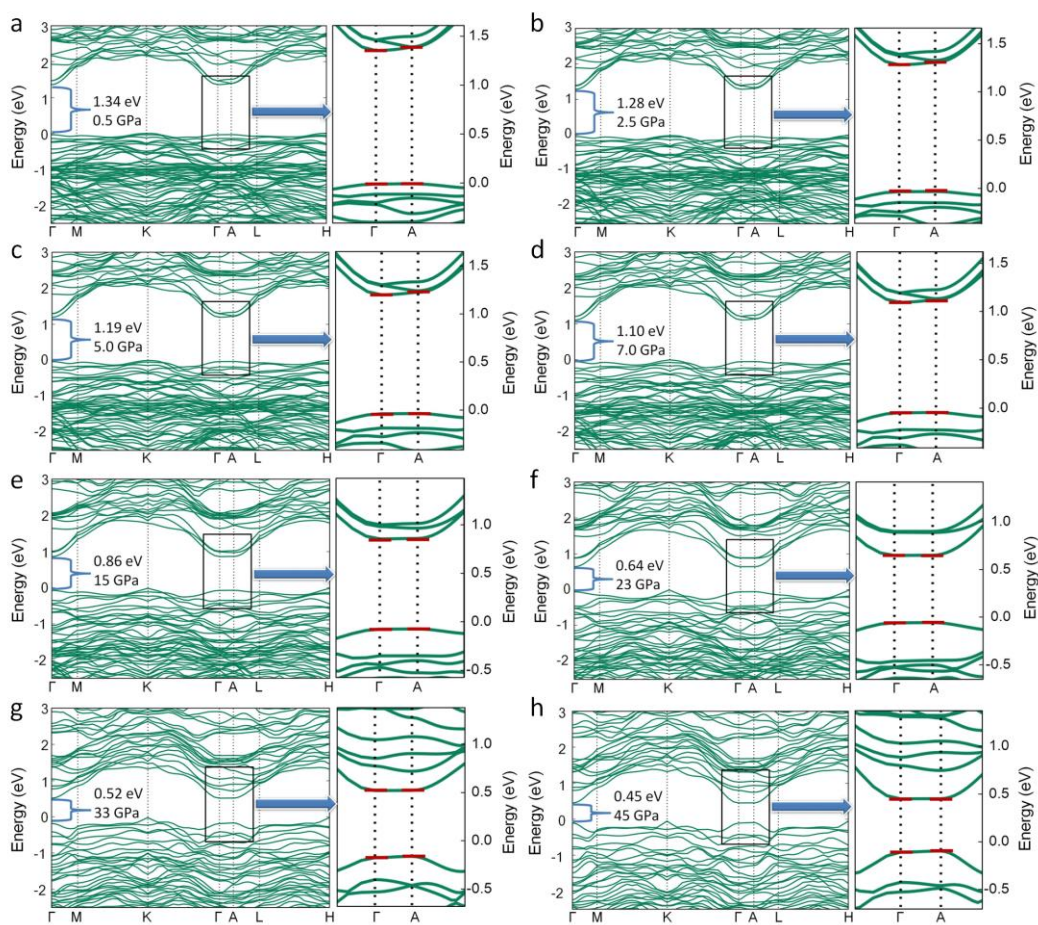


Table S1.

Refined structure parameters and selected bond lengths of the $\text{Bi}_9\text{O}_{7.5}\text{S}_6$ phases at low pressure (0.5 GPa) and high pressure (25.7 GPa).^a

Atom	x	y	z	$U_{\text{iso}} (\times 100 \text{ \AA}^2)$	g^a
<i>R-3m</i> (0.5 GPa)					
Bi1	0.3333	0.6667	0.6667	0.628(1)	1
Bi2	0.3333	0.6667	0.4568(1)	0.517(4)	1
S1	1	0	0.6148(5)	1.661(5)	1
O1	0.6667	0.3333	0.4824(15)	1.579(1)	1
O2	1	0	0.5	1.792(3)	0.5
Selected bond lengths					
Bi1—S1	2.808(1)				
Bi2—O1	2.109(1)	Bi2—O1	2.405(1)	Bi2—O2	2.693(4)
<i>R-3m</i> (25.7 GPa)					
Bi1	0.3333	0.6667	0.6667	0.552(1)	1
Bi2	1	0	0.7798(1)	0.931(4)	1
S1	1	0	0.5969(4)	1.640(7)	1
O1	0.6667	0.3333	0.8333(3)	1.515(1)	1
O2	1	0	0.8506(6)	1.911(6)	0.5
Selected bond lengths					
Bi1—S1	2.595(3)	Bi2—S1	2.925(2)		
Bi2—O1	1.745(1)	Bi2—O1	2.459(5)	Bi2—O2	2.622(1)

^aNumbers in parentheses are standard deviations of the last significant digit. U_{iso} is the isotropic thermal parameter, g is the occupation factor. R_{wp} and R_p are agreement indices for the structure refinements by the Rietveld method. At 0.5 GPa, space group *R-3m* (No 166): $a = b = 4.0437(2) \text{ \AA}$, $c = 30.8878(3) \text{ \AA}$ and $V = 438.83(3) \text{ \AA}^3$; $R_{\text{wp}} = 3.43\%$, $R_p = 2.40\%$; At 22.7 GPa, space group *R-3m* (No 166): $a = b = 3.7794(2) \text{ \AA}$, $c = 28.5252(1) \text{ \AA}$ and $V = 352.87(4) \text{ \AA}^3$; $R_{\text{wp}} = 3.40\%$, $R_p = 2.61\%$.